Numerical investigation of heat conduction in heterogeneous media with a discrete element method approach

H. Haddad, W. Leclerc, G. Alhajj Hassan, A. Ammar, Christine Pelegris, M. Guessasma, E. Bellenger

Version of Record: https://www.sciencedirect.com/science/article/pii/S1290072920312424
Manuscript_ff72ae7fd74eb62f3b63b72012ad0566

Numerical investigation of heat conduction in heterogeneous media with a discrete element method approach

H. Haddad, W. Leclerc, G. Alhajj Hassan, A. Ammar, C. Pélegris, M. Guessasma, E. Bellenger

Laboratoire des Technologies Innovantes, EA 3899, UPJV, 48 rue d'Ostende, IUT de l'Aisne, 02100 Saint Quentin, France

Abstract

Composite materials have been widely used across industry sectors. However, they are characterized by a variability of thermal conductivity with the architecture and manufacturing processes. Hence, thermal transfer in composite materials requires an improved fundamental understanding. From numerical purposes, the Finite Element Method (FEM) seems a robust method to study heat transfer in composite material. However, it does not establish a high-fidelity with the real life of material since it is difficult to take into account potential damage matrix or interface imperfection by this method. As such, this paper discusses the development of numerical approach based on the Discrete Element Method (DEM) to study heat transfer in composite materials. For that purpose, we consider a hybrid lattice model based on the equivalence between a particulate domain and a continuous medium. Several works have used the DEM to study heat transfer in a homogeneous and continuous medium. Through this contribution, we aim to extend this approach to investigate composite materials. The model is then validated in terms of temperature by comparison with numerical and experimental results through several applications. Furthermore, a special care taken in the evaluation of the heat flux density fields. To the knowledge of the authors, previous works did not interest to the examination of heat flux density when using the DEM. Indeed, this sensitive to the packing configuration and consequently always heterogeneous even if there typically homogeneous. To overcome this problem, an original smoothing technique called Halo is proposed and discussed in this work. Results exhibit the relevance of the proposed approach to evaluate both temperature and heat flux density fields with a good degree of precision compared with th FEM, the Fast Fourier Transformer (FFT) based method and experimental data.

Keywords: Discrete element method, heat conduction, effective thermal conductivity, thermal heat flux

1. Introduction

The number of applications of composite materials in the industry has increased significantly in recent years, due to low manufacturing costs as well as the customization of their mechanical and thermal properties. For example, when silica particles are added into a polymer matrix, they play an important role in improving electrical, mechanical and thermal properties of resulting composites [2]. Due to their complex microstructures, the detailed study of heat transfer turns out to be an arduous task. Therefore, technical analyses potentially focus on the macroscopic behaviour of such materials, dictated by effective properties such as ETC. The determination of the latter according to microstructural characteristics, individual phase properties and other relevant physical parameters is consequently of scientific and practical importance. For example, Chauhan et al. [3] studied the effect of geometry of filler particles on the effective thermal conductivity in the context of polymer composites. Mishra et al. [4] investigated on the effect of particle size on the thermal properties and void content of solid glass microsphere filled epoxy composites. Thus, considerable experimental works have been reported on the subject of thermal conductivity in composites. Among this vast literature, numerous studies have focused on the influence of filler volume fraction. For

example, Tavman [5] experimentally evaluated ETC of reinforced polyethylene composites as function of tin powder filler. Wong et al. [6] led experimental tests to determine ETC and effective elastic properties of epoxy resin with different kinds of inclusions as silica, alumina and aluminum fillers. Liang et al. [7] measured experimentally ETC of aluminum powder-filled phenol–aldehyde composites and graphite powder-filled phenol–aldehyde composites with filler volume fraction from 0 to 50 %. Boudenne et al. [8], investigated combined effects of inclusion concentration and size in the context of a polypropylene matrix filled with aluminum and copper fillers.

Many theoretical models [9] have also been developed to predict the ETC of composites. Among them, the Maxwell scheme [10] is considered to be one of the best homogenization technique due to its applicability to cases of multiphase composites. It predicts effective conductivities for dilute random sphere systems and a low volume fraction typically less than 25%. The method developed by Gandarilla-Pérez et al. [11] enabled to extent the classical Maxwell's homogenization to different geometrical shapes of inclusions. Authors also refer today to the Rayleigh sphere model [12] which includes thermal interaction between the particles to enhance Maxwell's model. Besides, Bruggeman [13] developed the Effective Medium Theory (EMT) which covers a wide range of materials, and Agari et al. [14] developed a model based on a generalization of parallel and series conduction models. Wong et al. [6] verified that both schemes are more accurate than Maxwell model for a high ratio of filler in the context of SiO_2/epoxy composite. Nielsen [15] proposed a modified Halpin-Tsai equation based on the generalized Einstein coefficient and a constant related to the relative conductivity of the phases. EMT , Agari model and Nielsen model were compared in the case of a Si_3N_4/epoxy composite [16]. Results exhibit that EMT and Nielsen model better predict ETC for a filler concentration lower than the range of 15–20%, 25–30% respectively but Agari model is more suited for a higher volume fraction. Khan et al. [17] developed a theoretical model to predict ETC of two-phase particulate composites containing highly conductive inclusions. More recently, in [18], is presented an efficient method for predicting the effective thermal conductivity of various types of two-component heterogeneous materials. Finally, it is acknowledged that the third order model discussed by Beasley and Torquato [19] enables to compute ETC of 2-phase particulate composite with a higher degree of precision, whatever the volume fraction of filler and the relative conductivity. Nevertheless, such a scheme takes benefit of a three-point parameter which requires very costly numerical computations to be accurately determined [20].

Moreover, several numerical approaches treated heat transfer by conduction and most of them focused on the ETC of composites [21, 22]. Typically, researchers take benefit of the Finite Difference Method (FDM) [23, 24] and the FEM [25, 26, 27] to attend their objectives. Thus, the FDM presented in [23] is suitable for calculating the ETC of mixed solid materials for different shapes of phases. It was also developed in [24] to predict the ETC of dendritic mushy zones as a function of fraction solid. The FEM was investigated in [28] to study heat conduction in heterogeneous materials with varying volume fraction, shape and size of fillers. The finite approach was also used in [27] to calculate the ETC of polymer composites with filler content ranging from 2.35 to 26.8 %. In , a numerical study using the FEM is proposed to However, other approaches also exist to determine ETC. For example, a numerical method based on FFT was developed to evaluate the effective properties of composite with periodic microstructure composed of constituents with linear or nonlinear mechanical behaviour [29, 30]. Besides, the DEM has also been applied is such a context [31, 32, 33, 34]. Indeed, this latter naturally accounts for discontinuities and is all well-suited to deal with a large spectrum of multi-scale and multiphysical phenomena. This approach originally developed by Cundall [35] to treat issues in rock mechanics field has been later applied to numerous problems, from the silo discharge [36] to the tribology of the wheel-rail contact [37] through the defect diagnosis in ball bearings [38, 39] and the simulation of crack propagation in continuous media [40, 41, 42]. Besides, a DEM based model was also investigated to simulate heat transfer by conduction in particulate systems using a contact conductance model introduced at the scale of the elementary inter-particular bond [31, 43, 44]. A similar approach based on the Finite Discrete Element Method (FDEM) is presented in [45]. Other works used a similar paradigm to consider heat transfer by conduction in continuous media using the concept of representative element [32, 33, 34]. Thus, some authors [32, 34] explored the benefit of a Voronoï tessellation to associate a well-defined polyhedron to each particle while other researchers considered Platonic solids

[33] for the same purpose. Furthermore, DEM has also proved its ability to simulate the thermo-elastic behavior of continuous materials as well as the thermal induced damage due to thermal expansion mismatch in continuous heterogeneous media [46, 47, 48].

The objective of this contribution is to study the ability of the DEM to simulate heat transfer by conduction in a continuous and heterogeneous 3D media. For this purpose, we consider a model based on the equivalence between a particulate system and a continuous media. In such an approach, the duality between particulate and lattice descriptions enables to introduce heat transfer by conductionbetween each pair of particles in contact using the natural inter-particular link. Thus, section and thermal properties associated to each contact manage the heat transfer by conduction through the entire 3D domain. Besides, we use the concept of representative element in which each discrete element is represented by a solid polyhedron with a number of faces equal to its number of neighbors. Thus, it is possible to provide proper transmission surface to each contact and a suitable mass to each particle. Due to limitations exhibited by Platonic solids which do not ensure conservation of mass and the high computational cost of the generation of Voronoï tessellations, we propose a third approach based on the calibration of transmission surface under the hypothesis of the equality between local and global conductivities. Furthermore, we are also interested in determining the heat flux field in 3D heterogeneous media. In DEM, this latter is typically heterogeneous even if this is theoretically homogeneous. In order to tackle such a difficulty, we propose to handle and adapt the Halo approach [49] recently developed to better evaluate the distribution of local stress in the context of linear elasticity. Please notice that, in this work, granular packings are generated using Lubachevsky-Stillinger Algorithm (LSA) [50] which enables an accurate control of intrinsic parameters such as the compacity, the size of particles and the coordination number which is defined as the average number of contacts per DE. All simulations are carried out using the house-built parallel MULTICOR3D++ code [51].

The present paper is outlined as follows. In Section 2, the numerical modeling based on the DEM is described and validated for a homogeneous media by comparison with analytical solutions. The estimation of the heat transmission surface between two particles based on a numerical calibration is also presented. In Section 3, we introduce the Halo approach to better evaluate the heat flux field distribution in a homogeneous media. In Section 4, we perform validation tests in the context of a single-inclusion composite. Comparisons are performed with analytical and other numerical approaches in terms of ETC, temperature and heat flux fields using the Halo approach. In Section 5, we discuss the case of a heterogeneous media, namely epoxy resin filled with ceramic fillers. ETC of the heterogeneous media is evaluated using the discrete approach and compared with analytical, numerical and experimental results. Afterwards, the heat flux is investigated, and comparisons with FEM are set up.

2. Heat transfer in continuous domain

In this section, we present a numerical approach based on the DEM to model thermal conduction in a continuous and homogeneous 3D media. The latter consists of a polydisperse particulate packing which can be considered as an Equivalent Continuous Medium (ECM) under several assumptions related to the arrangement of particles. For this purpose, intrinsic parameters such as the coordination number, the compacity and the polydispersity are controlled by the LSA. Besides, the isotropy of the particulate system is preliminary verified according to the process described by Leclerc et al. [30, 51] using statistical tools as the polar plots or the 2-point probability function to ensure that the effective properties are independent of direction. For information purposes, a volume fraction close to 0.64 and an average coordination number Z of 6.2 are typical of a 3D system of monodisperse particles. However, in the present work, we have deliberately chosen an average coordination number equal to 7.5 to ensure that each particle is at least in contact with 2 particles locally. This corresponds to the generation of new contacts and allows for a denser network of contacts. Moreover, the particle's radius follows a Gaussian distribution law and the dispersion is described by a ratio between the standard deviation and the average radius set to 0.3 in order to avoid possible directional effects.

2.1. DEM-based approach

In the proposed approach, we associate a representative element to each particle of the particulate system. Please notice that we are not interested in the shape of this element but rather in its characteristics such as volume and heat transmission surfaces. Thus, the volume of each representative element is chosen in order to satisfy the mass conservation hypothesis. In this purpose, the sum of the volumes of the representative elements must be equal to the volume of the studied domain. To do this, the mass of each particle is adjusted to the mass of the corresponding representative element by ϕ the volume fraction of the particulate system. If ρ_c [kg/m^3] is the density of the continuous material, the density of the particulate packing ρ_d [kg/m^3] can then be related to ρ_c via the following relation:

$$\rho_c = \phi \rho_d \tag{1}$$

The heat flux $W_{p,q}$ [W] transmitted by the transmission surface $S^t_{p,q}$ [m^2] between two representative elements (Figure 1) associated to particles p and q in contact, is defined as follows:

$$W_{p,q} = H^{p,q}_c (T_q - T_p) \tag{2}$$

where T_p, T_q are the temperatures of particles p, q and $H^{p,q}_c$ [W/K] is the thermal conductivity coefficient given by:

$$H^{p,q}_c = \frac{\lambda S^t_{p,q}}{d_{p,q}} \tag{3}$$

with λ the thermal conductivity of material and $d_{p,q}$ the distance between the centers of p and q. Thus, the heat transfer by conduction equation associated to each particle is:

$$C^d_p \frac{dT_p}{dt} + \sum_{q=1}^{n_p} W_{p,q} = Q^{tot}_p \tag{4}$$

with

$$C^d_p = C \rho_d V_p / \phi \tag{5}$$

where Q^{tot}_p [W] represents the external heat flux associated to particle p, n_p is the number of particles in contact with particle p, V_p is the volume of particle p and C represents the specific heat of the constitutive material. The temporal resolution of Equation (4) can be achieved by two types of numerical schemes (implicit or explicit). Implicit numerical patterns are stable for large steps of time. However, because of the large number of particles in contact, implicit numerical schemes are too expensive. As a result, our choice was to use an explicit numerical scheme that does not require an iterative procedure. The time discretization of Equation (4) leads to:

$$T^{t+\Delta t}_p = T^t_p + \frac{\Delta t}{C \rho_d V_p} \underbrace{\left[Q_p + \sum_{q=1}^{n_p} \frac{S^t_{p,q} \lambda}{d_{p,q}} (T^t_q - T^t_p) \right]}_{Q^{tot}_p} \tag{6}$$

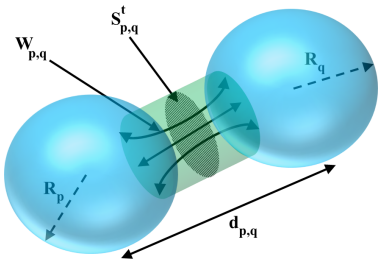

Fig. 1: Heat transfer by conduction at the contact scale

Calibration process

Unlike the FEM, for which the local properties at the finite element scale are identical to the macroscopic properties for a homogeneous media, local properties and parameters in discrete approach must be correlated to macroscopic properties. In the present work, the estimation of the heat transmission surface between two particles in contact is obtained by calibration. This choice is less expensive compared to approaches that are based on the generation of representative elements from a Voronoï decomposition of the domain [32]. It also ensures the conservation of the mass contrary to the approach based on Platonic solids [33]. In our case, the thermal conductivity of the equivalent medium depends on $S^t_{p,q}$ the transmission surface between two representative elements. We chose to correlate $S^t_{p,q}$ to a coefficient C_t and a surface $S_{p,q} = \pi R^2_m$ deducted from R_m the mean radius of the contact particles so that the expression of $S^t_{p,q}$ is:

$$S^t_{p,q} = C_t S_{p,q} \tag{7}$$

Thus, the thermal conductivity of the material is directly related to C_t coefficient without any dimensional effect. The latter is calibrated in order to obtain an equality between the thermal conductivity of the material and that considered at the contact scale. To do this, we proceed as follows. A heat flux φ is applied to the upper surface of the sample of length L, in the Y direction while a constant temperature T_0 is applied to the lower surface. The conditions under which the test is performed are described in Figure 2.

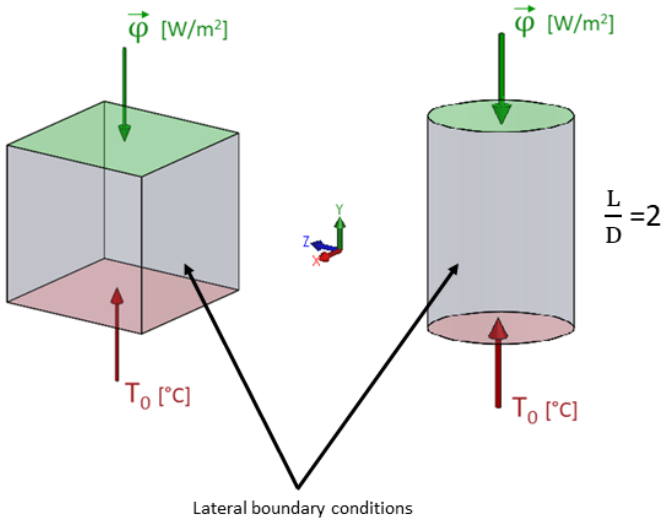

Fig. 2: Numerical test for the calibration process

For simplicity purposes, calculations are first performed using an arbitrary C_t (C^{arb}_t) set to 1. At the stationary state, a temperature difference ΔT is determined at the top surface and the ETC of the material

λ^e is deducted from the following equation:

$$\lambda^e = \frac{\varphi L}{\Delta T} \tag{8}$$

Finally, C_t coefficient is deducted from the following equality:

$$\frac{C_t}{C_t^{arb}} = \frac{\lambda}{\lambda^e} \tag{9}$$

We have evaluated C_t for a large range of density number which reaches 8000000 DE for cubic and cylindric configurations. Each data is obtained considering a number of 4 realizations. The variation of C_t is shown in Figure 3. C_t is found between 0.75 and 0.84. It depends on the number of particles and there is little effects of the geometry. The dispersion of results is characterized by the Coefficient of Variation (CoV) which is defined as the ratio of the standard deviation to the mean value. Since the CoV is less than 0.2% whatever the number of particles, we can conclude that we don't need calibration for a granular packing with a volume fraction close to 0.64 and an average coordination number Z of 7.5.

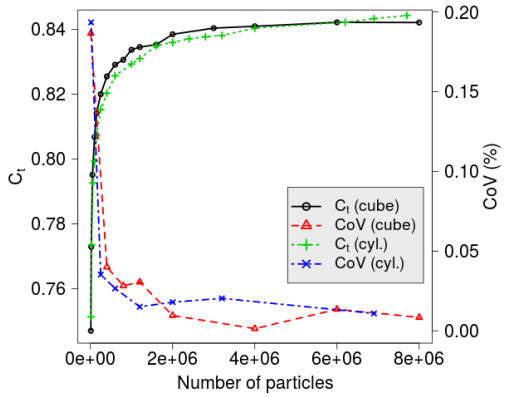

Fig. 3: Variation of C_t coefficient as function of DE number and geometry shape

Time step calculation

Based on the Equation (6), the explicit time integration for an interior particle p can be expressed as:

$$T_p^{t+\Delta t} = T_p^t + \frac{\alpha \Delta t}{V_p} \sum_{q=1}^{n_p} \frac{S_{p,q}^t}{d_{p,q}} (T_q^t - T_p^t) \tag{10}$$

where $\alpha = \frac{\lambda}{C\rho_d}$ designates the thermal diffusivity of the constitutive material. The explicit scheme is not unconditionally stable and the largest permissible value of the time step Δt is limited by a stability criterion. The time integration step is then limited by a critical time step Δt_{cr}. We assume that $S_{p,q}^t \approx C_t \pi R_m^2$, $V_p \approx \frac{4}{3}\pi R_m^3$ and $d_{p,q} \approx 2R_m$ with R_m the mean radius of particles. Furthermore, for a local coordination number n_p, Equation (10) simplifies to :

$$T_p^{t+\Delta t} \approx T_p^t + \frac{\alpha \Delta t}{\frac{4}{3}\pi R_m^3} \sum_{q=1}^{n_p} \frac{C_t \pi R_m^2}{2R_m} (T_q^t - T_p^t) \tag{11}$$

Moreover, Equation (11) can be rearranged as:

$$T_p^{t+\Delta t} \approx T_p^t + \frac{3C_t\alpha\Delta t}{8R_m^2}\sum_{q=1}^{n_p}(T_q^t - T_p^t) \tag{12}$$

We now define a dimensionless Fourier number τ as:

$$\tau = \frac{3C_t\alpha\Delta t}{8R_m^2} \tag{13}$$

It characterizes the part of the heat flux transmitted to a body at a given time t compared to the heat stored by the body. Then, we can reduce Equation (4) to:

$$T_p^{t+\Delta t} \approx T_p^t + \tau\sum_{q=1}^{n_p}(T_q^t - T_p^t) = (1-\tau n_p)T_p^t + \tau\sum_{q=1}^{n_p}T_q^t \tag{14}$$

The stability criterion requires that the coefficient multiplied by T_p^t in the $T_p^{t+\Delta t}$ expression must be greater or equal to zero [52]. Thus, $(1-\tau n_p) \geq 0$ or $\tau \leq \frac{1}{n_p}$. The integration time step is deduced :

$$\Delta t \leq \frac{8R_m^2}{3C_t\alpha n_p} \tag{15}$$

The critical time step Δt_{cr} for the solution of a thermal problem can be estimated by :

$$\Delta t_{cr} = \frac{2(d_{p,q}^{min})^2}{3\alpha n_p C_t} \tag{16}$$

with $d_{p,q}^{min}$ the minimal interparticle distance.

2.2. Validation of the DEM-based approach

In this section, we propose to validate the model in the context of a homogeneous media by comparison with an analytical solution. To do this, we consider a cubic pattern of length $L = 10$cm composed of $100,000$ spherical and polydisperse particles. This density of DE is a good compromise to ensure the isotropy of the particulate system and the accuracy of results while keeping a reasonable computational cost. C_t coefficient for this configuration is set to 0.806 according to the previous study. The pattern is subject to the following thermal conditions:

$$\begin{cases} T_1 : T(y=0) = 25°C \\ T_2 : T(y=\mathrm{L}) = 35°C \\ t=0 : T(y) = T_0 = 25°C \qquad 0 < y < \mathrm{L} \end{cases}$$

Besides, the lateral boundaries are under adiabatic conditions (Figure 4) and the material properties are given in Tab. 1:

Density	ρ_c	7800	kg/m^3
Thermal conductivity	λ	33	W/(mK)
Specific heat	C	0.9	J/(kgK)

Tab. 1: Material properties

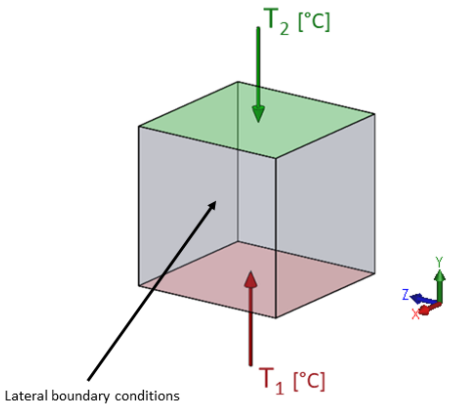

Fig. 4: Thermal conditions applied to the cubic pattern

The full development of the analytical resolution is detailed in [53]. The temperature field at any point is given by the following equation:

$$T(y) = T_1 + \frac{y\Delta T}{\mathrm{L}} + \Delta T \sum_{n=1}^{\infty} C_n \sin\left(\frac{n\pi y}{\mathrm{L}}\right) \quad e^{-\left(\frac{n\pi}{\mathrm{L}}\right)^2 \frac{\lambda t}{\rho C}} \tag{17}$$

where $C_n = 2 \times \frac{(-1)^n \times (1-\theta_0)+\theta_0}{n\pi}$ and θ_0 is defined as a dimensionless quantity: $\theta_0 = \frac{T_0 - T_1}{T_2 - T_1}$.

The temperature variation obtained by the analytical solution and the DEM after 0.05s, 0.1s and 0.2s is represented graphically in Figure 5-a. The results provided by the DEM are in good agreement with the analytical solution with a maximum relative error equal to 0.7 % (Figure 5-b). This validates the proposed formulation in the context of a homogeneous media.

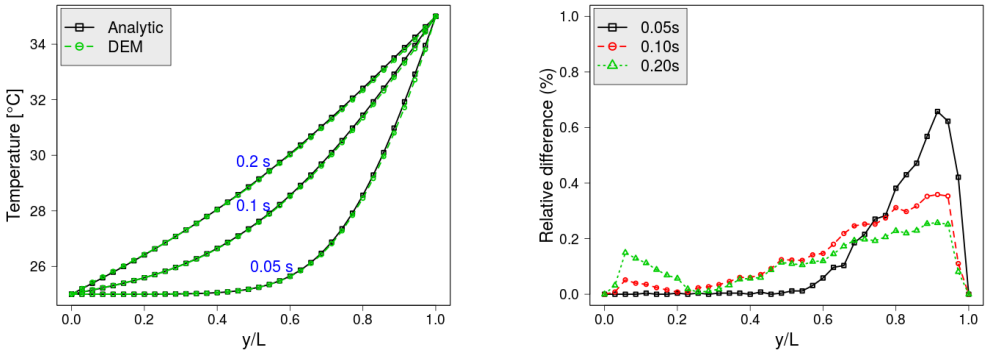

(a) (b)

Fig. 5: Comparison between analytic and discrete model solutions at several times for temperature as function of position y/L (a) and relative errors (b)

A second validation test is performed in order to prove the efficiency of the proposed approach. We have considered a spherical pattern with diameter $D = 10cm$ composed of aluminum. The initial temperature is $T_0 = 20°C$. The sphere is subjected to a constant temperature of $T_i = 200°C$ at the external surface. The specific heat is assumed to be 900 J/(kgK) . The thermal conductivity of the material is equal to 185 W/(mK) while the considered density is 2700 Kg/m^3. The conditions under which the test is performed are

described in the figure below. $C_t = 0.806$ when considering granular packing with 100000 DE and $C_t = 0.834$ for granular packing composed of 1 million DE.

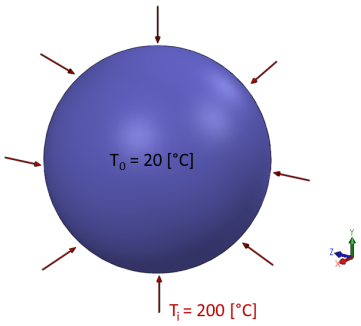

Fig. 6: Thermal conditions applied to a spherical sample

The analytical solution is given by the following equation:

$$T(r,t) = T_0 + \frac{2(T_0 - T_i)}{\pi r} \sum_{n=1}^{\infty} \frac{(-1)^n}{n} sin(\frac{n\pi r}{R}) e^{-\frac{a(\pi n)^2 t}{R^2}} \tag{18}$$

where r is the distance of the studied point from the center of the sphere and R is the radius of the sphere. The temperature T_c at the center of the sphere at time t is obtained when r approaches zero. It is expressed as:

$$T_c(t) = T_0 + 2(T_0 - T_i) \sum_{n=1}^{\infty} (-1)^n e^{-\frac{a(\pi n)^2 t}{R^2}} \tag{19}$$

Comparisons are made between the DEM with 100000 and 1 million particles, and analytical solution and FEM calculation with 100000 tetrahedral finite elements. In Figure 7. We have plotted the evaluation of the temperature at the center of the sphere. Results indicate that DEM matches closely to both analytical solution and the FEM calculations.

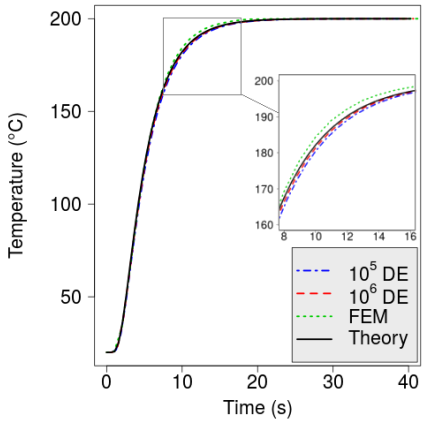

Fig. 7: Evolution of the temperature at the center of the sphere.

Figures 8-a and 8-b illustrate respectively the temperature fields at time $t = 10s$ of DEM model with 100000

DE and 1 Million respectively. The absolute difference between the DEM with 100000 DE and analytical solution is presented in Figure 8-c. Its exhibits a good agreement between the DEM and the analytic solution with max absolute difference less than of $1.93°C$ located at the center of the sphere. This highlights the suitability of the presented DEM-based approach in the present context.

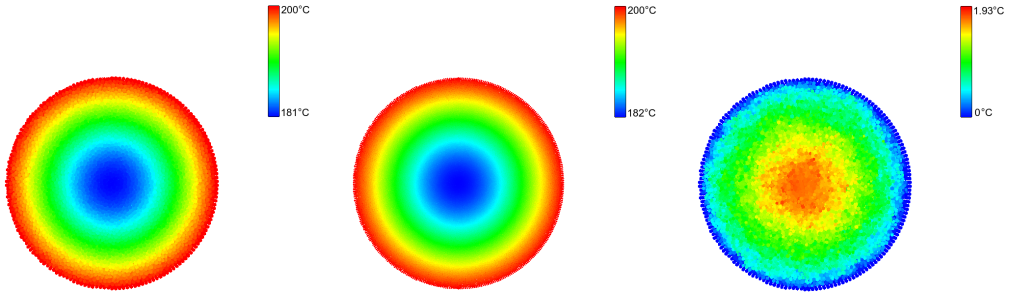

(a) (b) (c)

Fig. 8: Temperature profile of DEM model at time $t = 10s$ with 100000 DE (a) and 1 million DE (b) and absolute difference between the DEM with 100000 DE and analytical solution (c)

3. Halo approach to evaluate the heat flux

In a stationary state, the expression of the heat flux φ_p^i applied to a particle p is defined as below:

$$\varphi_p^i = \frac{\phi}{2V_p} \sum_{q \in Z_p} \underbrace{\left[\lambda S_{p,q}^t (T_q - T_p)\right]}_{\phi_{p,q}} e_{p,q}^i \tag{20}$$

where V_p is the volume of the particle, Z_p is the set of particles linked to the particle p and $e_{p,q}^i$ is the component of the inter-particle normal vector corresponding to i direction. In discrete simulations, due to the limited size and the randomness of the set of inter-particular contacts associated to each DE, the heat flux field is always heterogeneous even if it is theoretically homogeneous. In a first study, the case of a homogeneous media is addressed in order to determine the level of dispersion due to fluctuations at the particle scale. For this purpose, the same thermal conditions as described in Subsection 2.2 are imposed with a thermal conductivity set to 33 W/(mK). Thus, for a temperature difference ΔT equal to $10°C$ and a length $L = 10$cm, we should obtain an average heat flux equal to 3,300 W/m^2 according to the equation below:

$$\varphi = \frac{\lambda \Delta T}{L} \tag{21}$$

For a set of particulate packings ranging from 100,000 to 500,000 DE, the process is carried out and the heat flux density field is determined in order to evaluate the CoV corresponding to each test.Whatever the density of particles, a CoV about 27 % is found which describes a high level of dispersion. As a solution, we propose to adapt the Halo approach introduced by Moukadiri et al. [49] in the context of the stress field determination to evaluate the heat flux (Figure 9).

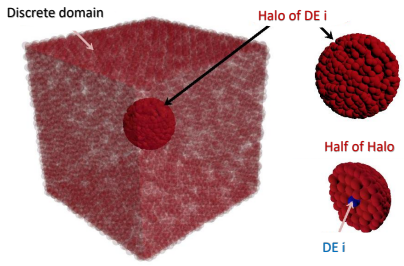

Fig. 9: Illustration of the Halo approach at the mesoscopic scale

More precisely, at the mesoscopic scale, a Halo of spherical shape is introduced for every DE. The center of DE is supposed to also be that of its Halo. This latter has a radius R_{Halo} and contains a pre-defined number of DE. The heat flux of a particle p is evaluated at the scale of Ω_p the Halo volume in order to take into account the contributions of the particles in the neighborhood of p. The expression of the heat flux applied to p is then:

$$\varphi_p^i = \frac{1}{2\Omega_p} \sum_{r \in \Omega_p} \sum_{q \in Z_r} \varphi_{r,q} e_{r,q}^i \tag{22}$$

with

$$\Omega_p = \frac{1}{\phi} \sum_{r \in \Omega_p} V_r \tag{23}$$

where Z_r is the set of particles linked to the particle r and V_r is the volume of particle r. One of the important questions deals with the choice of the suitable size of Halo. In this context, for a large spectrum of Halo-DE radius ratios, CoV is evaluated for two particulate packings of 100,000 and 500,000 DE. Results illustrated in Figure 10 exhibit that the level of dispersion is reduced for a higher Halo radius but is not influenced by the global density of particles. The user can easily determine the Halo radius corresponding to an expected heat flux distribution. A first indicator level at 5% is reached for a Halo-DE radius ratio close to 4. A second indicator at 2 % is reached for a Halo radius eleven times the radius of the DE. Besides, maximum, minimum and mean values in the discrete simulations are showed in Figure 11 compared with the expected value of heat flux.

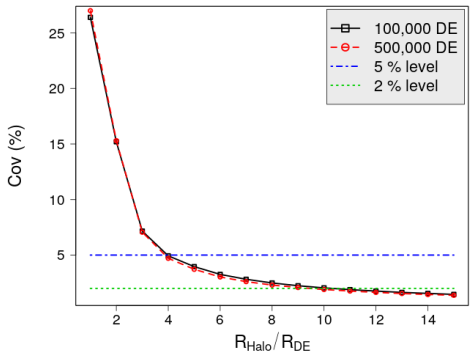

Fig. 10: Evolution of CoV as function of Halo size

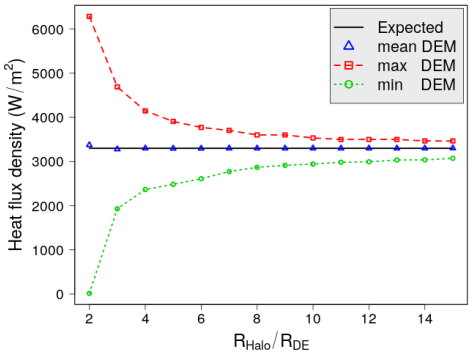

Fig. 11: Influence of Halo size on flux density: maximum, minimum and mean values

From this scope of results, we can see that whatever the Halo size, mean values are very close to the analytical one. One can notice a convergence of the maximum and minimum values to the analytical one. The lower fluctuations correspond to the larger Halo size. In addition, the normalized heat flux is illustrated in Figure 12 for different Halo radii. We can notice that the level of dispersion reduces for a larger Halo radius.

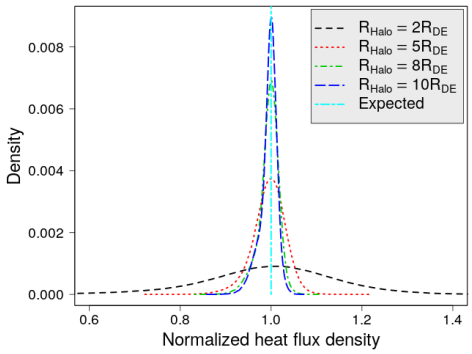

Fig. 12: Density functions of heat flux normalized by the average heat flux using different R_{Halo}

4. Single inclusion problem

We now aim to study the validation of the proposed approach in the context of a continuous and heterogeneous material. To attend this objective, we consider the example of a biphasic material modeled by a cubic pattern composed of a single inclusion of spherical shape embedded in a matrix. We consider a cubic pattern of length $L = 10$cm and a spherical inclusion of radius $a = \frac{L}{3}$ (Figure 13). Thus, the volume fraction of inclusion is equal to 15.51%.

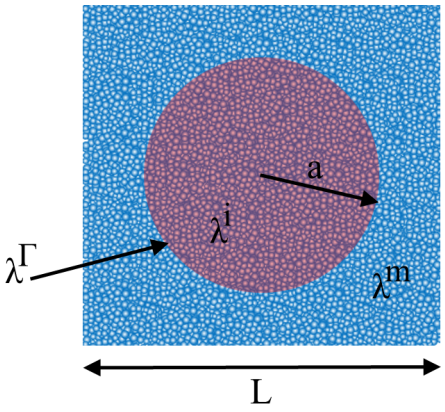

Fig. 13: Single-inclusion composite

4.1. ETC

The numerical test is performed using a particulate packing composed of 150,000 particles which is a good compromise between accuracy and computational cost. λ^i and λ^m are respectively the thermal conductivities of the inclusion and matrix phases. The case where two particles in contact are not located in the same phase, which typically corresponds to contacts located at the matrix-inclusion interface Γ, is treated specifically. From a numerical standpoint, this interface is supposed to be perfect and without thermal barrier. In this context, the thermal conductivity associated to the contact zone between both particles is averaged. In this work, we consider the following inverse average:

$$\lambda^\Gamma = \frac{2\lambda^i\lambda^m}{\lambda^i + \lambda^m} \tag{24}$$

This choice is justified by preliminary studies which showed that the arithmetic mean overestimates the ETC [32]. The specific heat is assumed to be 0.9 J/(K.kg) for both phases but this has little importance as long as this section focuses on the stationary state results. $c_\lambda = \frac{\lambda^i}{\lambda^m}$ refers to the contrast of thermal properties between the matrix and the inclusion. Several numerical tests are performed for property contrasts varying from 0.01 to 100. Comparisons, in terms of ETC, with the FEM and the analytical Maxwell model are performed and presented in Figure 14. Regardless of the contrast, less or greater than 1, the results obtained by the DEM are close to those obtained by the FEM and the Maxwell model. The maximum relative error is in the order of 0.65%. This highlights the ability of the DEM to estimate the ETC in this context.

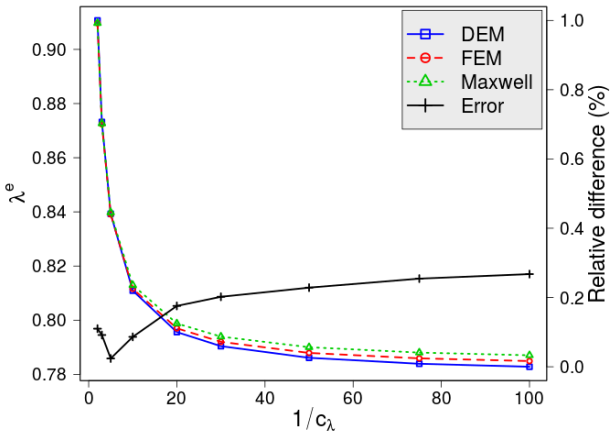

(a) $c_\lambda < 1$

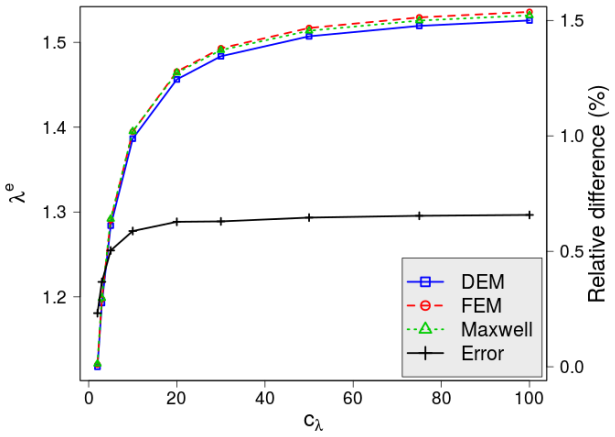

(b) $c_\lambda > 1$

Fig. 14: Single inclusion problem: non-dimensional thermal conductivity as a function of the contrast of properties

4.2. Temperature and heat flux fields

The thermal conductivities of the matrix and the inclusion are now fixed respectively to 33 and 165 W/(mK), so that the contrast of properties c_λ is equal to 5. For the same configuration and thermal conditions, comparisons with FEM in terms of temperature and heat flux are set up. For information purposes, FEM calculations are performed using a structured mesh composed of 100,000 4-node tetrahedral elements. Figure 15 illustrates the temperature field obtained by (a) the DEM and (b) the FEM. One can assume that both methods represent a quasi-identical temperature field. Figure 15-c illustrates the relative differences on temperature, based on linear interpolation functions, with respect to the FEM calculations. Numerical comparisons exhibit a quite good agreement between the DEM and the FEM calculations with relative differences less than 1%. Heat flux is also studied using Equation (22) with a Halo-DE radius ratio of 11 which corresponds to a 2% indicator level according to Figure 10. Figure 16 illustrates the heat flux fields obtained by the DEM (a) and the FEM (b). From a qualitative standpoint, they show that the results obtained by the DEM are in good agreement with the FEM. Please notice that the results presented in this section are taken in the XY cutting plane with Z = 0.5L. From a quantitative standpoint, the temperature and heat flux values extracted at positions A(0.5L,0.5L,0.5L), B(0.08L,0.5L,0.5L) and C(0.5L,0.92L,0.5L) are very close (Table 2). The relative differences on heat flux with respect to FEM calculation are presented in Figure 16-c with a maximum relative difference of 19.6%. This one is due to the approximation of heat flux at the inclusion/matrix level and adiabatic boundary conditions. The results obtained show that DEM

offers the possibility of estimating the heat flux field in a heterogeneous continuous media. According to these results, we can estimate that a particulate packing composed of 150,000 DE is suitable to represent the studied single-inclusion composite. Therefore, we estimate that a number of particles close to 23,000 DE is sufficient to represent a spherical inclusion.

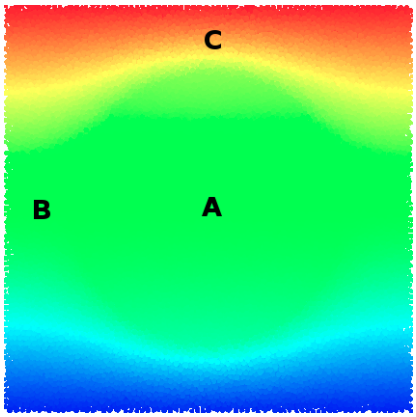

(a) DEM

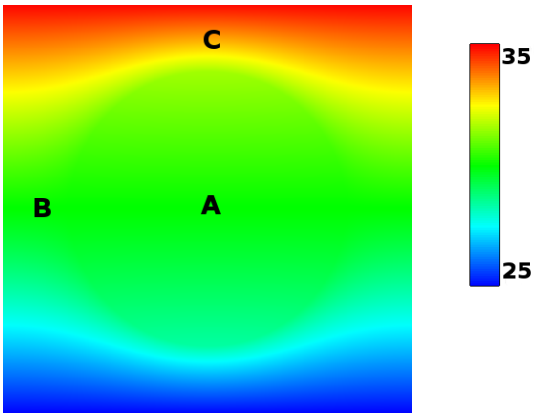

(b) FEM

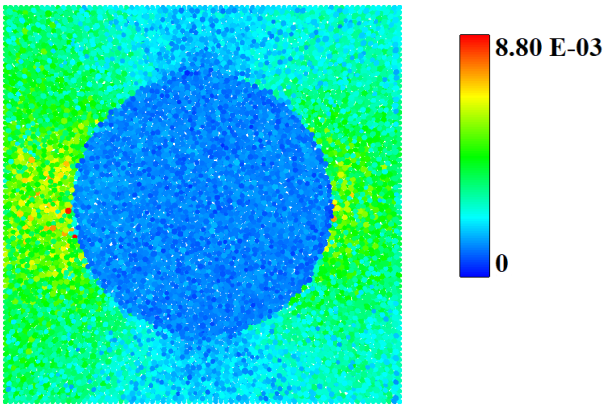

(c) Relative difference

Fig. 15: Single inclusion problem: temperature profile of DEM (a) and FEM (b) models and relative differences (c)

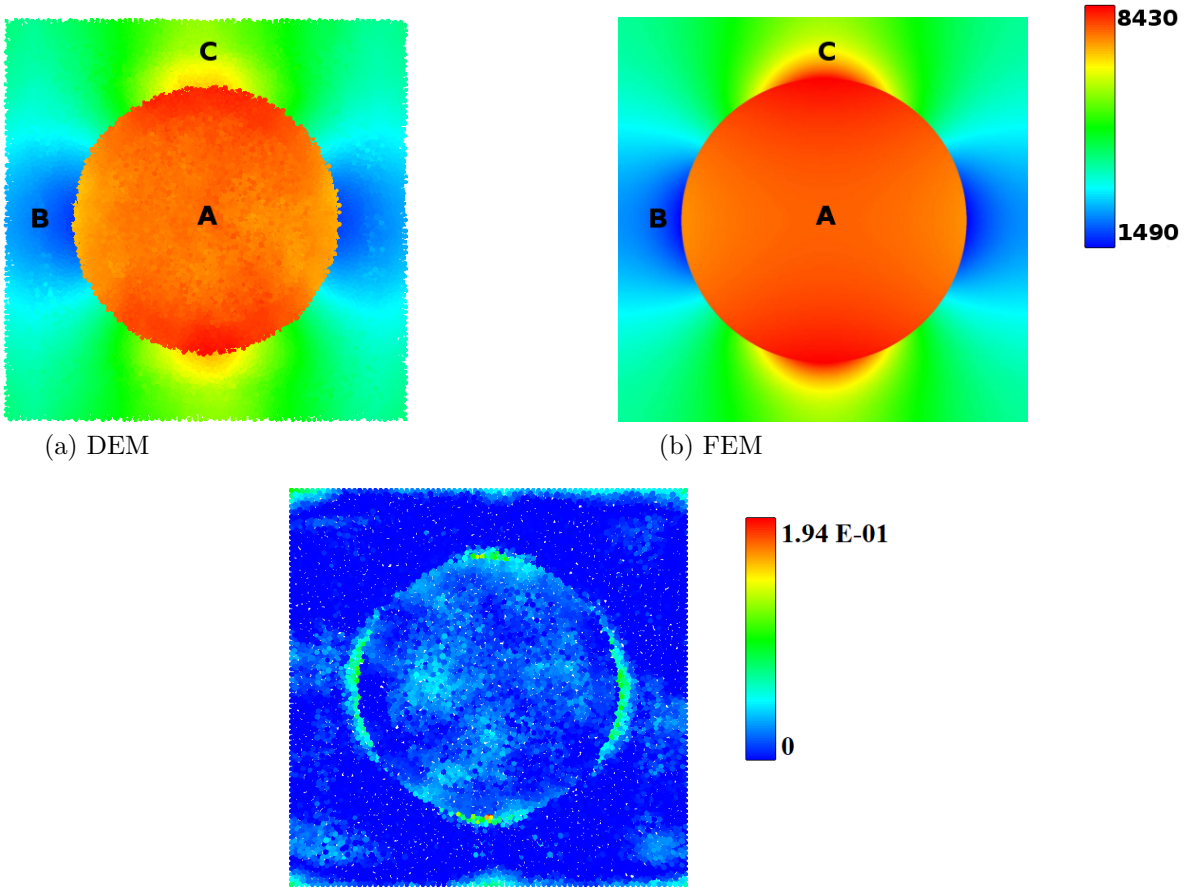

(a) DEM (b) FEM

(c) Difference

Fig. 16: Single inclusion problem: Heat flux profile [W/m^2] of DEM (a) and FEM (b) models and relative differences (c)

		position A	position B	position C
Temperature (°C)	150,000 DE	30	30	33.5
	500,000 DE	30	30	33.4
	FE	30	30	33.5
Heat flux (W/m^2)	150,000 DE	7796	2370	6183
	500,000 DE	7809	2342	6163
	FE	7767	2318	6424

Tab. 2: Temperature and heat flux values at A, B and C positions

5. Application to the case of a multi-inclusion composite material

This part focuses on a multi-inclusion composite material composed of an epoxy resin reinforced with ceramic fillers which was previously studied in [6]. Thermal conductivity values were determined using a utility software program at a stabilized mean sample temperature of 70 °C. Thus, ETC of composite was evaluated for a range of volume fraction of inclusions f_v from 0 to 50 % using different kinds of fillers. In this application, we are interested in fillers of silica with spherical shape. We should precise that the fillers of

silica studied by Wong et al. [6] were spherical polydisperse inclusions. For information purposes, thermal conductivity of epoxy is 0.195 W/(mK) and that of silica is 1.5 W/(mK) for a contrast of conductivities of 7.7. In a first step, we aim to compare the data obtained experimentally in term of ETC for different f_v to results provided by analytical and numerical methods. In a second step, numerical simulations are carried out to determine the heat flux distribution for a defined volume fraction of silica.

5.1. ETC

We first aim at evaluating ETC using the DEM and comparing results with other analytical, numerical and experimental values. We consider the following procedure. In a first step, a random set of dilute spherical inclusions is generated using LSA [50]. We limit our investigations to monodisperse inclusions and set the scale ratio between the length of the cubic pattern and the diameter of inclusions to 6. Thus, the number of fillers is directly governed by the targeted volume fraction. For information purpose, the length of the pattern L is set to 10cm but this has no influence on our results. The second steps consists in generating a dense enough particulate system to model the continuous medium. Based on the findings of Section 4, 23,000 DE are required to represent a spherical inclusion. Therefore, we can suppose that 8,000,000 DE can be considered enough to represent the medium where each spherical inclusion is modeled by about 20,000 DE. In a third step, the same thermal conditions are those cited in Subsection 2.2 are imposed. Finally, at the stationary state, the ETC is determined using the heat flux extracted from the numerical simulations and averaged. This process is carried out for a range of f_v from 10 to 50 % considering the thermal properties of the above-mentioned epoxy/silica composite. Figure 17 illustrates the results of the discrete approach with those obtained experimentally by Wong et al. [6] and compared with analytical results given by Maxwell and third-order models, and numerical ones obtained by FFT calculations using the Eyre-Milton scheme [54] and a regular grid composed of 134 millions of voxels ($512 \times 512 \times 512$ resolution). Relative errors between experimental and DE results are, at worse, close to 7 %. However, we hypothesize two explanations. First, the interface is assumed perfect without thermal barrier in our numerical simulations. Second, the polydispersity is not respected in numerical tests which could affect our results. Besides, relative differences with respect to the values given by the FFT-based approach are less than 0.5 % which highlights quite good adequation between DE and FFT approaches. From this scope of results, one can conclude that the DEM is able to predict the ETC of heterogeneous continuous media even with a high volume fraction of inclusions.

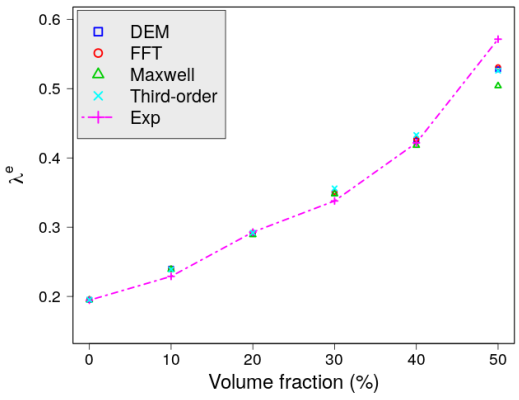

Fig. 17: ETC (W/(mK)) as a function of the volume fraction of silica

5.2. Temperature and heat flux fields

In this study, we consider the same configuration as previously but we limit our investigations to a volume fraction of silica of 20 % which corresponds to 83 spherical inclusions. For comparison purposes, numerical simulations are performed with DEM and FEM. In discrete approach, we handle the same particulate packing of 8,000,000 DE. In the Finite Element (FE) simulations, we consider a structured mesh composed of about 2,300,000 4-node tetrahedral elements to represent the multi-inclusion composite. At the stationary state,

the heat flux is determined by both approaches and results in the YZ plane with X = 0.5L are extracted and illustrated in Figure 18. For information purposes, the Halo-DE radius ratio is again set to 11 in discrete simulation. The results at positions A(0.5L,0.6L,0.6L), B(0.5L,0.02L,0.5L), C(0.5L,0.3L,0.55L) and D(0.5L,0.82L,0.87L) in terms of temperature and heat flux are reported in Table 3. This scope of results exhibits a quite good adequation between FE and DE approaches. Thus, relative errors with respect to the values given by the FEM are less than 3 % in terms of heat flux and 0.6 % for temperature values. This conclusion exhibits the ability of the DEM to simulate the heat conduction throughout such material at the steady state.

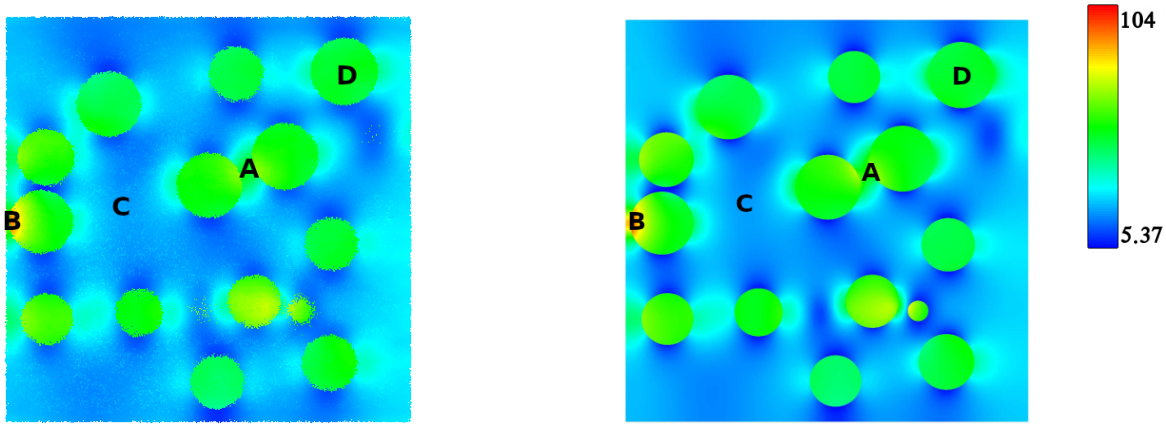

(a) DEM (b) FEM

Fig. 18: Heat flux (W/m^2) in the case of multi-inclusion composite using DE and FE approaches

		position A	position B	position C	position D
Temperature (°C)	DE	30.6	25.5	27.9	33
	FE	30.8	25.5	28	33.1
Heat flux (W/m^2)	DE	50.3	90.3	20.3	51
	FE	51.9	93.1	20.3	50.2

Tab. 3: Temperature and heat flux values at A, B, C and D positions

6. Conclusion

The numerical approach presented in this work showed the potential of the DEM to model heat transfer by conduction in a heterogeneous continuous media. In a first step, an approach based on the DEM was developed and validated in the case of a homogeneous continuum media. In a second step, the discrete approach was applied to the context of a single inclusion composite. Some comparisons were done with the FEM in terms of ETC and heat flux field. In a final step, a multi-inclusion composite, namely an epoxy resin filled with silica inclusions was modeled. DEM results were validated with experimental data found in the literature, the FFT-based approach and the FEM as function of volume fraction of silica. In all studied configurations, DEM showed its ability to model the heat transfer by conduction and to predict correctly even in heterogeneous media with a high fraction of inclusions its ETC. Furthermore, two original contributions can be highlighted. First, a calibration process was introduced to determine the transmission surfaces. Such an approach ensures the equality between local and global conductivities as well as the conservation of mass while avoiding the costly step of Voronoï tessellation. Secondly, due to local fluctuations inherent to the

DEM, we investigated a method to better evaluate the heat flux. Thus, the Halo approach was introduced to evaluate the heat flux at the scale of DE taking into consideration the contribution of DE located in its neighborhood. Results exhibited the capability of this concept. These fundamental conclusions pave the way of our future works. We look to combine Fourier and Fick law in order to model heat and mass transfer in heterogeneous media. Our ultimate goal is to provide an efficient and reliable numerical tool to simulate swelling and shrinkage mechanisms by adsorption and desorption of water. Furthermore, this numerical tool will be able to model thermal and hydric stresses and local damages in heterogeneous media.

Funding

The authors would like to gratefully acknowledge the European Union for the financial support under the INTERREG V France-Wallonie-Vlaanderen Program FWV N° 1.1.22.

Conflicts of interest

None declared.

References

[1] N. Moës and J. Dolbow T. Belytschko. A finite element method for crack growth without remeshing. *Numerical Methods in Engineering*, 46(1):131–150, 1999.

[2] R. Buchdahl. Mechanical properties of polymers and composites – vols. i and ii, lawrence e. nielsen, marcel dekker, inc., new york. *Journal of Polymer Science: Polymer Letters Edition*, 13(2):120–121, 1975.

[3] D. Chauhan, N. Singhvi, and R. Singh. Effect of geometry of filler particles on the effective thermal conductivity of two-phase systems. *The International Journal of Modern Nonlinear Theory and Application*, 2012.

[4] D. Mishra and A. Satapathy. An experimental investigation on the effect of particle size on the thermal properties and void content of solid glass microsphere filled epoxy composites. *IOP Conference Series: Materials Science and Engineering*, 115:012011, 2016.

[5] I.H. Tavman. Effective thermal conductivity of isotropic polymer composites. *International Communications in Heat and Mass Transfer*, 25(5):723 – 732, 1998.

[6] C. P. Wong and R. S. Bollampally. Thermal conductivity, elastic modulus, and coefficient of thermal expansion of polymer composites filled with ceramic particles for electronic packaging. *Journal of Applied Polymer Science*, 74(14):3396–3403, 1999.

[7] J. Z. Liang and G. S. Liu. A new heat transfer model of inorganic particulate-filled polymer composites. *Journal of Materials Science*, 44(17):4715–4720, 2009.

[8] A. Boudenne, L. Ibos, E. Géhin, M. Fois, and J. C. Majesté. Anomalous behavior of thermal conductivity and diffusivity in polymeric materials filled with metallic particles. *Journal of Materials Science*, 40(16):4163–4167, 2005.

[9] K. Pietrak and T.S. Wiśniewski. A review of models for effective thermal conductivity of composite materials. *J. Power Technol*, 95:14–24, 2014.

[10] J. Clerk Maxwell. *A Treatise on Electricity and Magnetism*, volume 2 of *Cambridge Library Collection - Physical Sciences*. Cambridge University Press, 2010.

[11] C.A. Gandarilla-Pérez, R. Rodríguez-Ramos, I. Sevostianov, F.J. Sabina, J. Bravo-Castillero, R. Guinovart-Díaz, and L. Lau-Alfonso. Extension of maxwell homogenization scheme for piezoelectric composites containing spheroidal inhomogeneities. *International Journal of Solids and Structures*, 135:125 – 136, 2018.

[12] L. Rayleigh Sec. R.S. On the influence of obstacles arranged in rectangular order upon the properties of a medium. *The London, Edinburgh, and Dublin Philosophical Magazine and Journal of Science*, 34(211):481–502, 1892.

[13] D. A. G. Bruggeman. Berechnung verschiedener physikalischer konstanten von heterogenen substanzen. i. dielektrizitätskonstanten und leitfähigkeiten der mischkörper aus isotropen substanzen. *Annalen der Physik*, 416(7):636–664, 1935.

[14] Y. Agari and T. Uno. Estimation on thermal conductivities of filled polymers. *Journal of Applied Polymer Science*, 32(7):5705–5712, 1986.

[15] L. E. Nielsen. The thermal and electrical conductivity of two-phase systems. *Industrial & Engineering Chemistry Fundamentals*, 13(1):17–20, 1974.

[16] H. He, R. Fu, Y. Han, Y. Shen, and X. Song. Thermal conductivity of ceramic particle filled polymer composites and theoretical predictions. *Journal of Materials Science*, 42(16):6749–6754, 2007.

[17] K. A. Khan, S. Z. Khan, and M. A. Khan. Effective thermal conductivity of two-phase composites containing highly conductive inclusions. *Journal of Reinforced Plastics and Composites*, 35(21):1586–1599, 2016.

[18] A. Seppälä. Efficient method for predicting the effective thermal conductivity of various types of two-component heterogeneous materials. *International Journal of Thermal Sciences*, 134:282 – 297, 2018.

[19] J. D. Beasley and S. Torquato. Bounds on the conductivity of a suspension of random impenetrable spheres. *Journal of Applied Physics*, 60(10):3576–3581, 1986.
[20] A. Gillman and K. Matous. Third order model of thermal conductivity for random polydisperse particulate materials using well-resolved statistical descriptions from tomography. *Physics Letters A*, 378, 2014.
[21] A. M. Thiele, A. Kumar, G. Sant, and L. Pilon. Effective thermal conductivity of three-component composites containing spherical capsules. *International Journal of Heat and Mass Transfer*, 73:177 – 185, 2014.
[22] H. Zhang, X. Ge, and H. Ye. Effectiveness of the heat conduction reinforcement of particle filled composites. *Modelling and Simulation in Materials Science and Engineering*, 13(3):401–412, 2005.
[23] Z. Yinping and L. Xingang. Numerical analysis of effective thermal conductivity of mixed solid materials. *Materials & Design*, 16(2):91 – 95, 1995.
[24] J. A. Spittle, K. Ravindran, and S. G. R. Brown. Numerical prediction of the effective thermal conductivity of dendritic mushy zones. *Modelling and Simulation in Materials Science and Engineering*, 7(1):59–70, 1999.
[25] M. Jiang, I. Jasiuk, and M. Ostoja-Starzewski. Apparent thermal conductivity of periodic two-dimensional composites. *Computational Materials Science*, 25(3):329 – 338, 2002.
[26] R. Nayak, D. P. Tarkes, and A. Satapathy. A computational and experimental investigation on thermal conductivity of particle reinforced epoxy composites. *Computational Materials Science*, 48(3):576 – 581, 2010.
[27] A. Agrawal and A. Satapathy. Computational, analytical and experimental investigation of heat conduction of particulate filled polymer composite. *Universal Journal of Mechanical Engineering 3.1*, 2015.
[28] A. Saini, S. Unnikrishnakurup, C.V. Krishnamurthy, K. Balasubramanian, and T. Sundararajan. Numerical study using finite element method for heat conduction on heterogeneous materials with varying volume fraction, shape and size of fillers. *International Journal of Thermal Sciences*, 159:106545, 2021.
[29] J.C. Michel, H. Moulinec, and P. Suquet. Effective properties of composite materials with periodic microstructure: a computational approach. *Computer Methods in Applied Mechanics and Engineering*, 172(1):109 – 143, 1999.
[30] W. Leclerc, N. Ferguen, C. Pélegris, H. Haddad, E. Bellenger, and M. Guessasma. A numerical investigation of effective thermoelastic properties of interconnected alumina/al composites using fft and fe approaches. *Mechanics of Materials*, 92:42–57, 2016.
[31] W. L. Vargas and J. McCarthy. Heat conduction in granular materials. *AIChE Journal*, 47:1052–1059, 2001.
[32] H. Haddad, W. Leclerc, and M. Guessasma. Application of the discrete element method to study heat transfer by conduction in particulate composite materials. *Modelling and Simulation in Materials Science and Engineering*, 26(8):085010, 2018.
[33] I. Terreros, I. Iordanoff, and J-L. Charles. Simulation of continuum heat conduction using DEM domains. *Computational Materials Science*, 69:46–52, 2013.
[34] M. Hahn, T. Wallmersperger, and B. Kroplin. Discrete element representation for the thermal field: Proof of concept and determination of the material parameters. *Computational Materials Science*, 50 (10):2771–2784, 2010.
[35] P. A. Cundall and O. D. L. Strack. A discrete numerical model for granular assemblies. *Géotechnique*, 29:235–257, 1979.
[36] F. Nicot, N. Hadda, M. Guessasma, J. Fortin, and O. Millet. On the definition of the stress tensor in granular media. *International Journal of Solids and Structures*, 2013.
[37] S. Descartes, M. Renouf, N. Fillot, B. Gautier, A. Descamps, Y. Berthier, and Ph. Demanche. A new mechanical–electrical approach to the wheel-rail contact. *Wear*, 265(9):1408 – 1416, 2008.
[38] C. Machado, M. Guessasma, and E. Bellenger. Electromechanical modeling by DEM for assessing internal ball bearing loading. *Mechanism and Machine Theory*, 92:338 – 355, 2015.
[39] C. Machado, M. Guessasma, and V. Bourny. Electromechanical prediction of the regime of lubrication in ball bearings using discrete element method. *Tribology International*, 127:69 – 83, 2018.
[40] Z. Chen, X. Jin, and M. Wang. A new thermo-mechanical coupled DEM model with non-spherical grains for thermally induced damage of rocks. *Journal of the Mechanics and Physics of Solids*, 116:54 – 69, 2018.
[41] S. Hentz, F. V. Donzé, and L. Daudeville. Discrete element modelling of concrete submitted to dynamic loading at high strain rates. *Computers & Structures*, 82(29):2509 – 2524, 2004.
[42] K. Radi, D. Jauffrès, S. Deville, and C. L. Martin. Elasticity and fracture of brick and mortar materials using discrete element simulations. *Journal of the Mechanics and Physics of Solids*, 126:101 – 116, 2019.
[43] Y. T. Feng, K. Han, C. F. Li, and D. R. J. Owen. Discrete thermal element modelling of heat conduction in particle systems: Basic formulations. *J. Comput. Physics*, 227:5072–5089, 2008.
[44] H.W. Zhang, Q. Zhou, H.L. Xing, and H. Muhlhaus. A DEM study on the effective thermal conductivity of granular assemblies. *Powder Technology*, 205(1):172 – 183, 2011.
[45] C. Joulin, J. Xiang, J-P. Latham, and C.C. Pain. Capturing heat transfer for complex-shaped multibody contact problems, a new fdem approach. *Computational Particle Mechanics*, 2020.
[46] D. André, M. Jebahi, I. Iordanoff, J.-L. Charles, and J. Néauport. Using the discrete element method to simulate brittle fracture in the indentation of a silica glass with a blunt indenter. *Computer Methods in Applied Mechanics and Engineering*, 265:136 – 147, 2013.
[47] W. Leclerc, H. Haddad, and M. Guessasma. On the suitability of a discrete element method to simulate cracks initiation and propagation in heterogeneous media. *International Journal of Solids and Structures*, 108:98 – 114, 2017.
[48] G. Alhajj Hassan, W. Leclerc, C. Pélegris, M. Guessasma, and E. Bellenger. On the suitability of a 3D discrete element method to model the composite damage induced by thermal expansion mismatch. *Computational Particle Mechanics*, 2019.
[49] D. Moukadiri, W. Leclerc, K. Kamel, Z. Aboura, M. Guessasma, E. Bellenger, and F. Druesne. Halo approach to evaluate the stress distribution in 3D discrete element method simulation : Validation and application to flax/bio based epoxy

composite. *Modelling and Simulation in Materials Science and Engineering*, (6):065005, 2019.
[50] B. D. Lubachevsky and F. H. Stillinger. Geometric properties of random disk packings. *Journal of Statistical Physics*, 60(5):561–583, 1990.
[51] W. Leclerc. Discrete element method to simulate the elastic behavior of 3D heterogeneous continuous media. *International Journal of Solids and Structures*, 121:86 – 102, 2017.
[52] Y. A. Cengel. *Heat and mass transfer: a practical approach, 3rd edn. McGraw-Hill, New York.* 2007.
[53] B. Weigand. *Analytical Methods for Heat Transfer and Fluid Flow Problems.* 2004.
[54] D. Eyre and G. Milton. A fast numerical scheme for computing the response of composites using grid refinement. *European Physical Journal. Applied Physics.*, 6:41 – 47, 1999.